Structural Engineering and Mechanics, *Vol. 53, No. 3 (2015) 607-623*
DOI: http://dx.doi.org/10.12989/sem.2015.53.3.607

Separation of background and resonant components of wind-induced response for flexible structures

Jing Li*, Lijuan Li and Xin Wang

Faculty of Civil and Transportation Engineering, Guangdong University of Technology, Guangzhou 510006, China

(Received June 11, 2013, Revised June 4, 2014, Accepted July 4, 2014)

Abstract. The wind-induced dynamic response of large-span flexible structures includes two important components-background response and resonant response. However, it is difficult to separate the two components in time-domain. To solve the problem, a relational expression of wavelet packet coefficients and power spectrum is derived based on the principles of digital signal processing and the theories of wavelet packet analysis. Further, a new approach is proposed for separation of the background response from the resonant response. Then a numerical example of frequency detection is provided to test the accuracy and the spectral resolution of the proposed approach. In the engineering example, the approach is applied to compute the power spectra of the wind-induced response of a large-span roof structure, and the accuracy of spectral estimation for stochastic signals is verified. The numerical results indicate that the proposed approach is efficient and accurate with high spectral resolution, so it is applicable for power spectral computation of various response signals of structures induced by the wind. Moreover, the background and the resonant response time histories are separated successfully using the proposed approach, which is sufficiently proved by detailed verifications. Therefore, the proposed approach is a powerful tool for the verification of the existing frequency-domain formulations.

Keywords: background response; large-span flexible structure; power spectral analysis; resonant response; wavelet packet transform; wind-induced response

1. Introduction

In the research field of structural wind engineering, the wind-induced response is usually divided into three parts: the mean response, the background component, and the resonant component. This processing method is widely used in wind-resistant analysis of structures and determination of equivalent static wind loads (Chen and Zhou 2007, Holmes 2002, Li *et al*. 2011, Yang *et al*. 2013), because the method helps to reveal the mechanism of wind effects on structures. As a basic method for wind-induced response analysis of structures, the frequency-domain method is based on linear assumptions and able to obtain the formulations for the power spectra of background response, resonant response, and total response, respectively. In a word, the frequency-domain representations of the three types of stochastic responses can be derived using this method.

*Corresponding author, Associate Professor, E-mail: leyking@163.com

http://www.techno-press.org/?journal=sem&subpage=8 ISSN: 1225-4568 (Print), 1598-6217 (Online)

It should be noted that the correctness of the frequency-domain theory needs to be validated due to the great efforts made to derive the formulations and develop the corresponding computer program. However, the subject of validating the frequency-domain method is seldom involved in literature. In particular, the problem of how to validate the power spectra formulations of background response and resonant response respectively remains unanswered. On the other hand, the frequency-domain method has obvious limitations. For example, this method is not applicable for the wind-induced response analysis of the spatial structures with large span, light weight, and complex shape. Under this circumstance, the time-domain method is employed to take into account the nonsteady and the nonlinear factors. The time-domain analysis results-the time histories of various responses-can be decomposed into the mean response and the fluctuating response. And then, by power spectral analysis of the fluctuating response samples, the energy distribution features of structural vibration can be shown and known. Since both the time-domain and the frequency-domain methods can result in the power spectra of the wind-induced responses, the comparison of the numerical results obtained by these two methods respectively is an effective approach to verification of the correctness of the frequency-domain method. As mentioned earlier, the three types of stochastic responses including the time histories of the background and resonant components are the source data for power spectral estimation when using the time-domain method. However, it is difficult to extract the time histories of the background and resonant components from the fluctuating response, which needs to be solved.

In order to validate the correctness of the frequency-domain method, the power spectral estimation of a stochastic response time history is an important step, and there are various kinds of methods for this purpose, in which the methods based on fast Fourier transform (FFT) are well established and widely utilized in engineering. However, the FFT-based methods have limitations, e.g., they are only applicable for steady signals and unable to give consideration to both the higher and the lower frequency components of the signal because the resolution is fixed. The theory of signal processing can be applied to wind-resistant analysis of engineering structures. According to the theory of stochastic vibration, the question of whether the structural response is stationary depends on the properties of the structural system and the excitation. For example, when a nonlinear structure is subjected to nonstationary wind loads, the stochastic response will be nonlinear and nonstationary (Clough and Penzien 2003). In such case the traditional FFT-based methods are not suitable for analysis. Fortunately, a new set of time-frequency analysis tools-the wavelet analysis methods-have been created and developed, which can be applied to structural wind engineering (Aksoy *et al*. 2004, Kitagawa and Nomura 2003, Terradellas and Morales 2001). The wavelet analysis provides an auto-adaptive time-frequency window, whose time scale is wider at a lower frequency band; in contrast, the time scale is narrower at a higher frequency band. Such features make the wavelet methods very suitable for time-frequency analysis of wind-induced response signals containing both stationary and nonstationary segments. It is known that the wavelet transform can be classified into the continuous wavelet transform, the discrete wavelet transform, and the wavelet packet transform. Compared with the other two types, the wavelet packet transform has the advantages such as fine division of frequency band and high efficiency. Moreover, as a type of time-frequency transform, it stores the necessary information in time-domain, so it enables us to extract the background and the resonant component time histories from a total response signal. Therefore, the wavelet packet transform is superior for the wind response analysis of large-span flexible structures.

In this paper, the relation between wavelet packet transform and power spectrum is derived based on the principle of digital signal processing and the theory of wavelet analysis. Further, a

new approach is proposed for separation of the background response from the resonant response. The proposed approach is applied to analysis of wind-induced response signals of a large-span roof structure, and the power spectra of various responses are obtained. Then the ratios of the background/resonant response variance to total-response variance are determined. Finally, the background and the resonant signals are extracted successfully from the fluctuating response signal. The above results prove the effectiveness of the proposed approach.

2. Fundamentals of wavelet packet analysis

A subspace U_j^n corresponding to frequency band n of layer j is defined as the closure space of the function $u_n(x)$, and let $u_n(x)$ satisfy the two-scale equations (Percival and Walden 2000)

$$\begin{cases} u_{2n}(x) = \sqrt{2}\sum_{k\in \boldsymbol{Z}} h_k u_n(2x-k) \\ u_{2n+1}(x) = \sqrt{2}\sum_{k\in \boldsymbol{Z}} g_k u_n(2x-k) \end{cases} \tag{1}$$

where $\{h_k\}$ and $\{g_k\}$ denote the coefficients of low-pass filter and the coefficients of high-pass filter, respectively. Using the above equations the spatial decomposition can be obtained

$$U_{j+1}^n = U_j^{2n} \oplus U_j^{2n+1} \qquad j \in \boldsymbol{Z}, n \in \boldsymbol{Z}_+ \tag{2}$$

The cluster of functions $\{u_n(x)\}$ constructed by Eq. (1) is called the wavelet packet which is determined by the basis function $\varphi(x)=u_0(x)$. The tree of wavelet packet decomposition is shown in Fig. 1.

For a given signal, Mallat's fast algorithm for wavelet packet decomposition is applied to compute the two series $\{d_l^{j,2n}\}$ and $\{d_l^{j,2n+1}\}$ from the known $\{d_l^{j+1,n}\}$

$$\begin{cases} d_l^{j,2n} = \sum_k h_{k-2l} d_k^{j+1,n} \\ d_l^{j,2n+1} = \sum_k g_{k-2l} d_k^{j+1,n} \end{cases} \tag{3}$$

where l, j, n are the parameters for translation, scale, and frequency band respectively, $d_l^{j,2n}$ and $d_l^{j,2n+1}$ are the wavelet packet coefficients in the subspaces U_j^{2n} and U_j^{2n+1} respectively, and h_{k-2l}, g_{k-2l} are the coefficients of low-pass and high-pass filters, respectively.

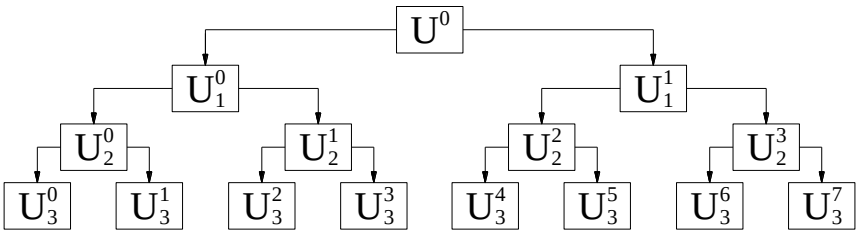

Fig. 1 Three-layer tree of wavelet packet decomposition

3. Time-domain method for wind-induced response analysis of structures

The substance of time-domain method for wind-induced response analysis is the nonlinear finite element analysis. The main steps are as follows:

(1) The wind pressure time series are obtained through the synchronous pressure measurement on a rigid model of the structure in an atmospheric boundary layer wind tunnel.

(2) The structure is discretized as finite elements, and wind pressure is applied to the corresponding element. Then the nodal displacement, velocity, and acceleration at each time-step are obtained by solving the differential equation of motion using the nonlinear finite element method.

(3) On the basis of the statistical analysis of various response samples, the mean, the root mean square (RMS) and the spectral feature of response (i.e., nodal displacement and element stress or force) can be obtained. Further, the rules of structural vibration are concluded.

The above steps are applicable to any structure subjected to any excitation and able to offer the whole-process information on structural dynamic response. Therefore the time-domain method is an effective approach for wind-induced response analysis of large-span flexible structures.

4. Formulation of power spectrum based on wavelet packet decomposition for stochastic signals

Let $f(t)$ be a stochastic process, which is sampled with time interval Δt to obtain the series $\{f_r\}$, where r is the time parameter. Setting $W=\exp(-\mathrm{i}2\pi/N)$, where i is the imaginary unit and N is the number of data points, the Fourier transform of $\{f_r\}$ is

$$F_k = \frac{1}{N}\sum_{r=0}^{N-1} f_r W^{kr}, \quad k = 0,1,\cdots,N-1. \tag{4}$$

The auto-correlation function of $\{f_r\}$ is

$$R_r = \frac{1}{N}\sum_{s=0}^{N-1} f_s f_{s+r} \tag{5}$$

where r is the time lag and $-(N-1)\le r\le N-1$.

According to the Wiener-Khintchine theorem, there is a relation of Fourier transform between the correlation function and the power spectrum of the signal, so the spectral density function of $\{f_r\}$ is

$$S(\omega) = \frac{1}{2\pi}\int_{-\infty}^{\infty} R(\tau)\exp(-\mathrm{i}\omega\tau)d\tau \tag{6}$$

where $R(\tau)$ is the correlation function.

The above equation needs discretization. Setting $\omega=k\Delta\omega$, $\tau=r\Delta t$ and $S_k=S(k\Delta\omega)\Delta\omega$, we can get

$$S_k = \frac{1}{N}\sum_{r=-(N-1)}^{N-1} R_r W^{kr}. \tag{7}$$

Substitution of Eq. (5) into Eq. (7) gets

$$S_k = \frac{1}{N}\sum_{s=0}^{N-1} f_s \frac{1}{W^{ks}}\left[\frac{1}{N}\sum_{r=-(N-1)}^{N-1} f_{s+r} W^{k(s+r)}\right]. \tag{8}$$

Let t=s+r, then

$$S_k = \frac{1}{N}\sum_{s=0}^{N-1} f_s\left[\frac{1}{N}\sum_{t=s-(N-1)}^{s+N-1} f_t W^{k(t-s)}\right]. \tag{9}$$

Because the time series $\{f_r\}$ is of finite length, the upper bound and lower bound of the second summation sign in the above equation can be modified to get

$$\begin{aligned} S_k &= \frac{1}{N}\sum_{s=0}^{N-1} f_s\left[\frac{1}{N}\sum_{t=0}^{N-1} f_t W^{k(t-s)}\right] \\ &= F_k F_k^* \end{aligned} \tag{10}$$

where F_k is the Fourier transform of $\{f_r\}$, and F_k^* denotes the conjugate complex number of F_k.

Eq. (10) gives a power spectral computation method based on FFT, whose limitation is that only the transform for frequency domain is used without any resolution of time domain. To solve the problem, a time-frequency analysis tool-the wavelet packet transform-will be introduced in the following.

There is Parseval's formula (Mitra 2001) for the energy conservation theorem

$$I = \int_R f^2(t)dt = \frac{1}{2\pi}\int_R \overline{\hat{f}(\omega)}\hat{f}(\omega)d\omega \tag{11}$$

where $f(t)$ is the stochastic process, $\hat{f}(\omega)$ represents the continuous Fourier transform of $f(t)$, ω represents the angular frequency component of $f(t)$, and the overline denotes the conjugate complex. Then dt is replaced by Δt, $d\omega$ is replaced by $\Delta\omega$, so $\hat{f}(\omega) = N\Delta t F_k$, and the above equation is written in the discrete form

$$I = \frac{\Delta\omega}{2\pi}\sum_{k=0}^{N-1}(N\Delta t)^2 F_k^* F_k = N\Delta t\sum_{k=0}^{N-1} S_k\ . \tag{12}$$

The wavelet packet decomposition with the layer j is applied to the signal $f(t)$, and $f(t)$ is expanded using the wavelet packet basis as

$$f(t) = \sum_{n=0}^{2^j-1}\sum_{k=1}^{N/2^j} c_{n,k} w_n^{j,k}(t) \tag{13}$$

where $c_{n,k}$ is the wavelet packet coefficient, and $\{w_n^{j,k}(t)\}_{k\in \mathbf{Z}}$ is the normalized orthogonal basis in the subspace U_j^n.

Substitution of Eq. (13) into Eq. (11) obtains

$$I = \int_R\left[\sum_n\sum_k c_{n,k} w_n^{j,k}(t)\right]^2 dt\ . \tag{14}$$

Using the orthogonal relations

$$\begin{aligned} \langle w_n^{j,k}(t),\, w_n^{j,l}(t)\rangle &= \delta_{kl} \\ \langle w_{2n}^{j,k}(t),\, w_{2n+1}^{j,l}(t)\rangle &= 0 \end{aligned} \tag{15}$$

where δ_{kl} is the Kronecker delta, Eq. (14) can be simplified as

$$I = \Delta t \cdot \sum_n \sum_k c_{n,k}^2 \,. \tag{16}$$

When the frequency range of the signal is divided finely, i.e., the value of j is large, the variation of S_k in each frequency band n ($0 \le n \le 2^j - 1$) is so small that it can be regarded as a constant G_n. Taking $G_n = \sum_k S_k / (N / 2^j)$, we can get the equation from Eq. (12)

$$I = N\Delta t \sum_{n=0}^{2^j-1} G_n \cdot \frac{N}{2^j} \,. \tag{17}$$

By wavelet packet decomposition of the signal to the layer j, the total energy of the signal can be decomposed into the energy components corresponding to the different frequency bands, then from Eqs. (16)-(17), the energy component corresponding to the frequency band n can be expressed as

$$\Delta t \sum_k c_{n,k}^2 = N\Delta t G_n \frac{N}{2^j} \,. \tag{18}$$

Therefore the power spectrum of the signal $f(t)$ is

$$G_n = 2^j \sum_k c_{n,k}^2 / N^2 \qquad n = 0,1,\cdots,2^j - 1 \,. \tag{19}$$

Eq. (19) offers a new form to express the power spectrum of stochastic signals, where the coefficient $c_{n,k}$ has two subscripts-the frequency band number n and the translation parameter k, which denote the frequency and the time, respectively. Using such advantage of time-frequency representation, the background and the resonant response time histories can be extracted from the response signal of the structure.

5. A numerical approach for separation of background component from resonant component

On the basis of the work of the above section, a new approach is proposed for separation of background component from resonant component in time domain. The detailed procedures are as follows:

(1) The wind-induced response analysis of structure is performed using the time-domain method.

(2) The wavelet basis function and the layer of wavelet packet decomposition are selected.

(3) The wavelet packet decomposition is applied to the displacement (or internal force) time history $f(t)$ of a node (or an element) to obtain the wavelet packet coefficients $c_{n,k}$, and the power

spectral density of the signal is determined by Eq. (19).

(4) The response time history $f(t)$ can be expressed as the summation of the mean response μ_f and the fluctuating response $\tilde{f}(t)$ with zero mean. Let f_s be the sampling frequency of $f(t)$, and then the frequency interval of power spectrum is $[0, \pi f_s]$ (rad/s). Further, the frequency dividing point ω_b between background response and resonant response is determined reasonably (Zhou and Gu 2010), which will be demonstrated by the engineering example. Let ω_b be located in the frequency band numbered n_b, and the background and resonant response time histories are obtained using the reconstruction technique of multiple frequency bands, namely

$$\begin{cases} \tilde{f}(t) = f_b(t) + f_r(t) \\ f_b(t) = \sum_{i=0}^{n_b} \sum_{k \in \mathbf{Z}} c_{i,k} \psi_i^{j,k}(t) \\ f_r(t) = \sum_{i=n_b+1}^{2^j-1} \sum_{k \in \mathbf{Z}} c_{i,k} \psi_i^{j,k}(t) \end{cases} \tag{20}$$

where $f_b(t)$, $f_r(t)$ denote the background and resonant response time histories, respectively, $c_{i,k}$ is the wavelet packet coefficient, $\psi_i^{j,k}(t)$ is the wavelet function, and i,j,k are the parameters for frequency band, scale, and translation, respectively.

(5) Procedures (3)-(4) are repeated for other node or element until the separations of background and resonant responses are finished for all the displacements of nodes or internal forces of elements of the structure.

6. Verification criteria for power spectral estimation of stochastic signals

The various signals in engineering can be classified into two types: the determinate signal and the stochastic signal. For a determinate signal, e.g., the sine or cosine signal, the spectral curve can be verified intuitively because only a few frequency components are contained. However, for a stochastic signal, it is difficult to judge the truth of the spectral curve, so a reasonable and effective method is required for verification of the power spectrum. Here two criteria based on the statistics of the signal are proposed.

(1) RMS criterion: the RMS obtained by the power spectrum should equal the standard deviation of the signal, i.e.

$$\left| \sqrt{\Delta\omega \cdot \sum_i S_i} - \mathrm{std}(\{f\}) \right| < \varepsilon_1 \tag{21}$$

where $\mathrm{std}(\{f\})$ is the standard deviation of structural response signal, $\{S_i\}$ is the spectral series, $\Delta\omega$ is the frequency increment, ε_1 is a small enough tolerance. If $\{f\}$ is the background or resonant response signal, the spectral curve for the background or resonant response can also be verified.

(2) Correlation function criterion: it is known from Eq. (6) that the correlation function values at different time lags can be obtained by inverse Fourier transform (IFT) of the power spectrum, and the value should equal that obtained by statistical analysis of the signal, i.e.

$$\left|\mathrm{IFT}\left(\{S_i\},r\right)-\frac{1}{N-r}\sum_{s=0}^{N-1-r}f_s f_{s+r}\right|<\varepsilon_2 \tag{22}$$

where IFT($\{S_i\}$,r) denotes the correlation function value at time lag r obtained by IFT of the series $\{S_i\}$, and ε_2 is a small enough tolerance.

7. A numerical example of frequency detection

The emulational signal is a combinative function with two frequencies which are very close to each other

$$s(t)=\sin(2\pi f_1 t)+\cos(2\pi f_2 t)$$

where f_1=1.5 Hz, f_2=1.56 Hz, and the sampling interval Δt=0.15s. The waveform of the signal is shown in Fig. 2. In the wavelet packet analysis, the coif4 wavelet function is used, and decomposition layer j=8. As a result, the spectrum is shown in Fig. 3.

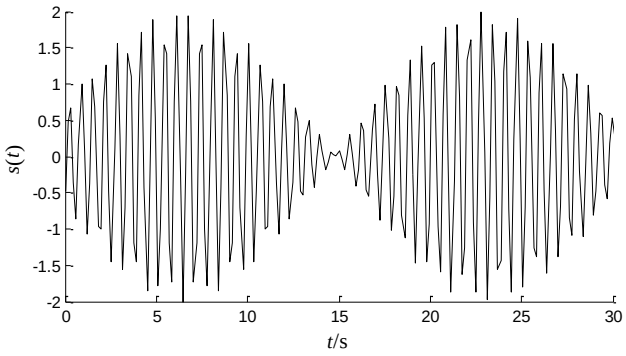

Fig. 2 Waveform of double-frequency signal

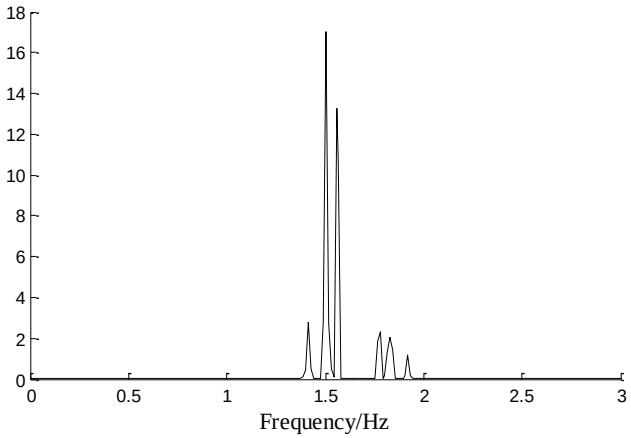

Fig. 3 Spectrum of double-frequency signal

Table 1 Results of frequency detection (Hz)

	Wavelet function	f_1	f_2
Given value		1.500	1.560
Detected value	coif4	1.504	1.556
	sym6	1.501	1.559

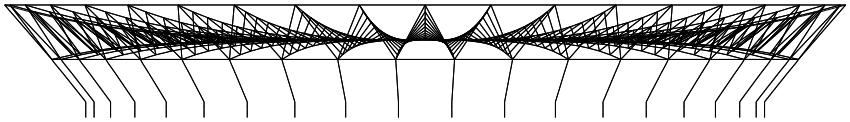

(a) Elevation

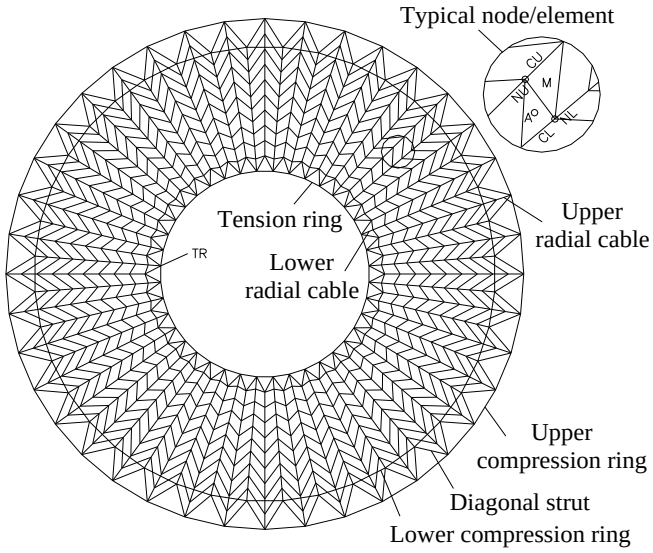

(b) Plan

Fig. 4 Cable-membrane structure

As seen in Fig. 3, the two highest spectral peaks corresponding to the two frequency components separate from each other distinctly, which indicates a high spectral resolution. Besides the detected frequency components, several small-amplitude side lobes are formed naturally. It can be known by analysis that the location of side lobe is relevant to the neighboring major frequency. Further, two wavelet functions are selected respectively to compute the spectrum, and comparisons of the given frequency and the detected value by spectral analysis are shown in Table 1. It is seen that the frequency components are detected accurately using the proposed approach.

8. Engineering example

The roof structure of the Foshan Century Lotus Stadium as shown in Fig. 4 is a typical tensile

Table 2 Lower-order natural frequencies of the cable-membrane structure

Order No.	1	2	3	4	5	6
Frequency (Hz)	0.7586	0.8690	0.8690	0.9658	0.9809	0.9809

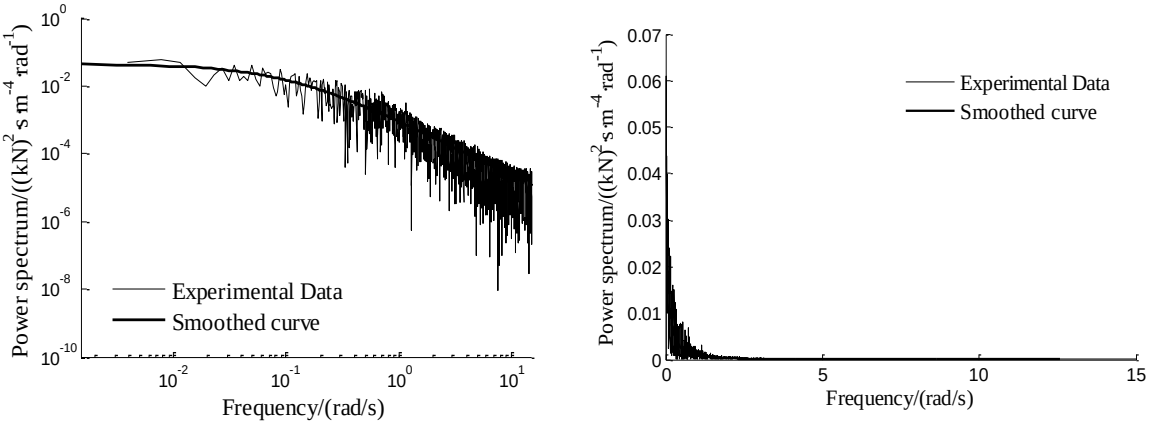

(a) Logarithmic scale (b) Linear scale

Fig. 5 Auto-spectrum of wind pressure acting on typical node A

cable-membrane structure. The horizontal projection is annular and covers 63000 m^2 with outside diameter of 310 m and inside diameter of 125 m. As the skeleton of the roof structure, a cable-net is composed by the inner tension ring, upper radial cables, lower radial cables, and hanger cables. Also, the difference in height of the two compression rings is 20 m. Therefore, a stable structural system is formed by the exterior compression rings, the interior tension ring, various cables, and membrane to carry deadweight and wind loading. The roof structure is connected to the infrastructure via 40 prestressed concrete pillars.

The wind pressure time histories acting on the prototype roof are obtained according to the wind tunnel experiment on the roof model (Wacker 2004). Form-finding analysis and wind-induced vibration analysis are performed using the Strand7 software, and the finite element model is shown in Fig. 4. Also, the lower-order natural frequencies are captured by modal analysis, shown in Table 2.

To investigate the power spectral characteristics of wind pressure, the auto-spectrum of the pressure acting on typical node A of the roof is plotted according to experimental data in Fig. 5. Further, the spectral curve is smoothed to show the tendency more clearly.

As shown in Fig. 5, the typical wind pressure spectrum is decreasing, whose energy is distributed on the lower frequency band of [0, ω_u], where ω_u is a proper upper cut-off frequency beyond which the spectral value is regarded as zero.

Using the proposed approach, the power spectra of the structural response are computed, and the background and resonant response time histories are extracted. The parameters are taken as: sampling interval Δt=0.2s, wavelet function is db5, and decomposition layer j=10. The results are given in the following.

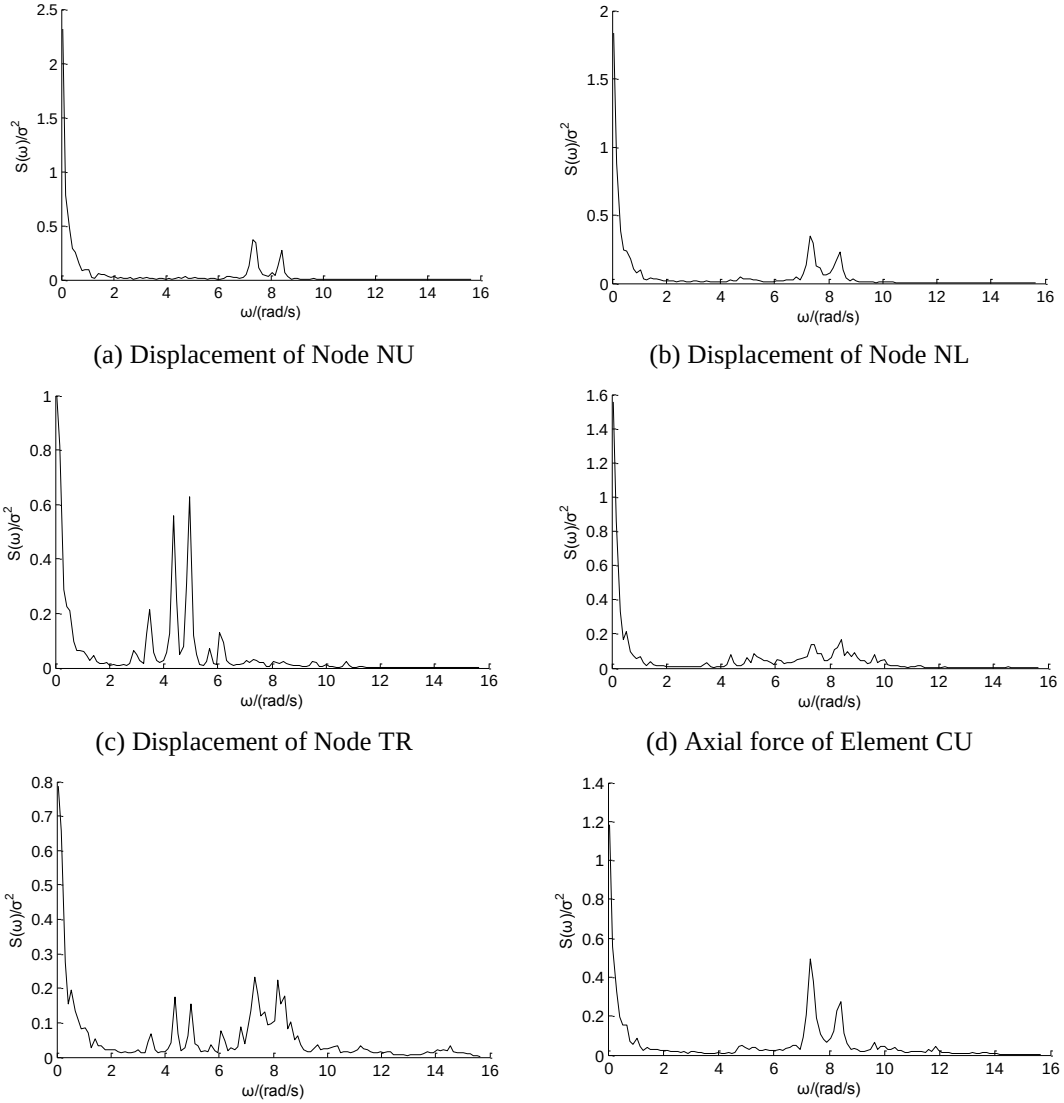

(a) Displacement of Node NU (b) Displacement of Node NL

(c) Displacement of Node TR (d) Axial force of Element CU

(e) Axial force of Element CL (f) Major principal stress of Element M

Fig. 6 Response power spectra of typical nodes and elements

8.1 Response power spectra

The response power spectra (variance-normalized spectra) of the typical nodes and elements (see Fig. 4) are shown in Fig. 6. Figs. 6(a)-(c) are displacement spectra, and (d)-(f) are internal force spectra.

As shown in Fig. 6, the spectral curves of the six types of responses are similar in shape: each curve can be divided into two parts, i.e., the monotone decreasing curve at lower frequency band and the small-amplitude spectral peaks at higher frequency band. Because structural displacements are the solutions of the equation of motion, the features of displacement power spectra provide

scientific basis for determination of the frequency dividing point ω_b between the background response and the resonant response. In order to determine the value of ω_b more reasonably, the following factors are considered:

(1) The displacement spectral curves shown in Figs. 6(a)-(b) are typical for the wind-induced response. It is noted that the shape of the monotone decreasing part of each displacement spectral curve is very similar to that of the wind pressure spectrum shown in Fig. 5, which indicates the quasi-static effect of the fluctuating wind pressure, namely the background response, so the point for ω_b should be located in the connection of the two parts of the spectral curve.

(2) The frequency band [0, ω_b] should contain most of the energy (e.g., 95%) of the wind pressure spectrum. In other words, ω_b can be regarded as the upper cut-off frequency ω_u of the wind pressure spectrum.

(3) By modal analysis of the structure (see Table 2) we know the first-order frequency $\omega_1=2\pi f_1=4.766$ rad/s, and ω_b should be less than ω_1.

Considering the above three factors we obtain the value of frequency dividing point as $\omega_b=4.50$rad/s.

8.2 Power spectral verification

The accuracy of the computed power spectrum is verified using the proposed criteria, shown in Table 3 and Fig. 7.

Table 3 Verification of RMS response

Response type	RMS	From power spectrum	From time history
Displacement of tension ring (m)	σ_b*	5.562E-02	5.577E-02
	σ_r	4.260E-02	4.222E-02
	σ	7.006E-02	6.995E-02
Axial force of upper radial cable (kN)	σ_b	119.4	118.8
	σ_r	104.7	104.2
	σ	158.9	158.0

*σ_b: The root mean square (RMS) of background response; σ_r: The RMS of resonant response; σ: The RMS of total response.

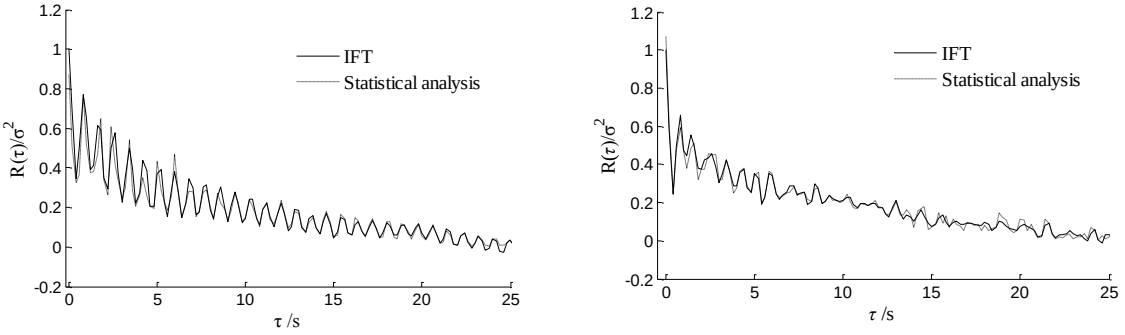

(a) Displacement of node of upper radial cable (b) Axial force of upper radial cable

Fig. 7 Verification of correlation functions

Table 4 Ratio of the background/resonant variance to total variance

Response type	σ_b^2/σ^2	σ_r^2/σ^2
Displacement of node of upper radial cable	0.653	0.347
Displacement of node of lower radial cable	0.630	0.370
Displacement of node of tension ring	0.683	0.317
Axial force of upper radial cable	0.572	0.428
Axial force of lower radial cable	0.477	0.523
Major principal stress of membrane	0.444	0.556

As seen in Table 3, the RMS response obtained by quadrature of power spectrum approximates the corresponding sample statistic. As shown in Fig. 7, the correlation function obtained by IFT of power spectrum coincides well with that from statistical analysis of sample. The above results indicate that the power spectrum computed by the proposed approach truly reveals the rules of energy distribution for the stochastic signal, i.e. the computed spectrum is accurate.

8.3 Background and resonant response time histories

We can get herein the ratio of background variance to total variance σ_b^2/σ^2 and the ratio of resonant variance to total variance σ_r^2/σ^2 based on the power spectra, shown in Table 4.

As seen in Table 4, the ratio of background/resonant variance to total variance varies with the response type. As stated previously, the displacement power spectra show the basic features of structural vibration, and the results of the three types of displacements indicate that the background response is primary, and that the resonant response is secondary for the large-span cable-membrane structure. This conclusion is consistent with that from the related research (Wu *et al*. 2008).

Before discussing the background response and the resonant response time histories, a residual is defined as

$$r_f(t) = \mu_f + f_b(t) + f_r(t) - f(t) \tag{23}$$

where μ_f is the mean response, $f_b(t)$ and $f_r(t)$ are the background and the resonant responses respectively, $f(t)$ is the total response, $r_f(t)$ is the residual.

The displacement sample of typical node NU is taken for example to verify the accuracy of the proposed approach. First, the background and resonant components are extracted from the total displacement time history using the proposed approach; second, the residual is computed by Eq. (23); third, the wavelet packet transforms are applied to the background and the resonant signals respectively, and the power spectra are computed by Eq. (19); finally, the results are plotted in Fig. 8.

As shown in Fig. 8, the residual is much less than any of the response time histories, so it is regarded as zero. In other words, the extracted background and resonant responses can be used to reconstruct the total response time history accurately. As for the spectral features of the two extracted components, it is seen that the power spectrum of the background response covers the lower frequency range of [0, 4.4792]. In contrast, the power spectrum of resonant response covers the higher frequency range of [4.4792, 12.088]. Both of the spectral curves of the extracted components coincide perfectly with the corresponding parts of the total-response spectrum. Therefore, it has been fully proved that the extracted time histories shown in Figs. 8(b)-(c) are in

truth the background and the resonant responses, respectively.

The total displacement time history of another typical node TR and the corresponding mean response, background component, and resonant component are shown in Fig. 9.

As shown in Figs. 8-9, the wind-induced response of structure has obvious nonstationary feature; the background response time history reflects the variational tendency of the fluctuating response (with zero mean) with time and has the low-frequency and nonstationary feature; in contrast, there are many sharp spikes in the resonant response time history, so the resonant response has the high-frequency and stationary feature.

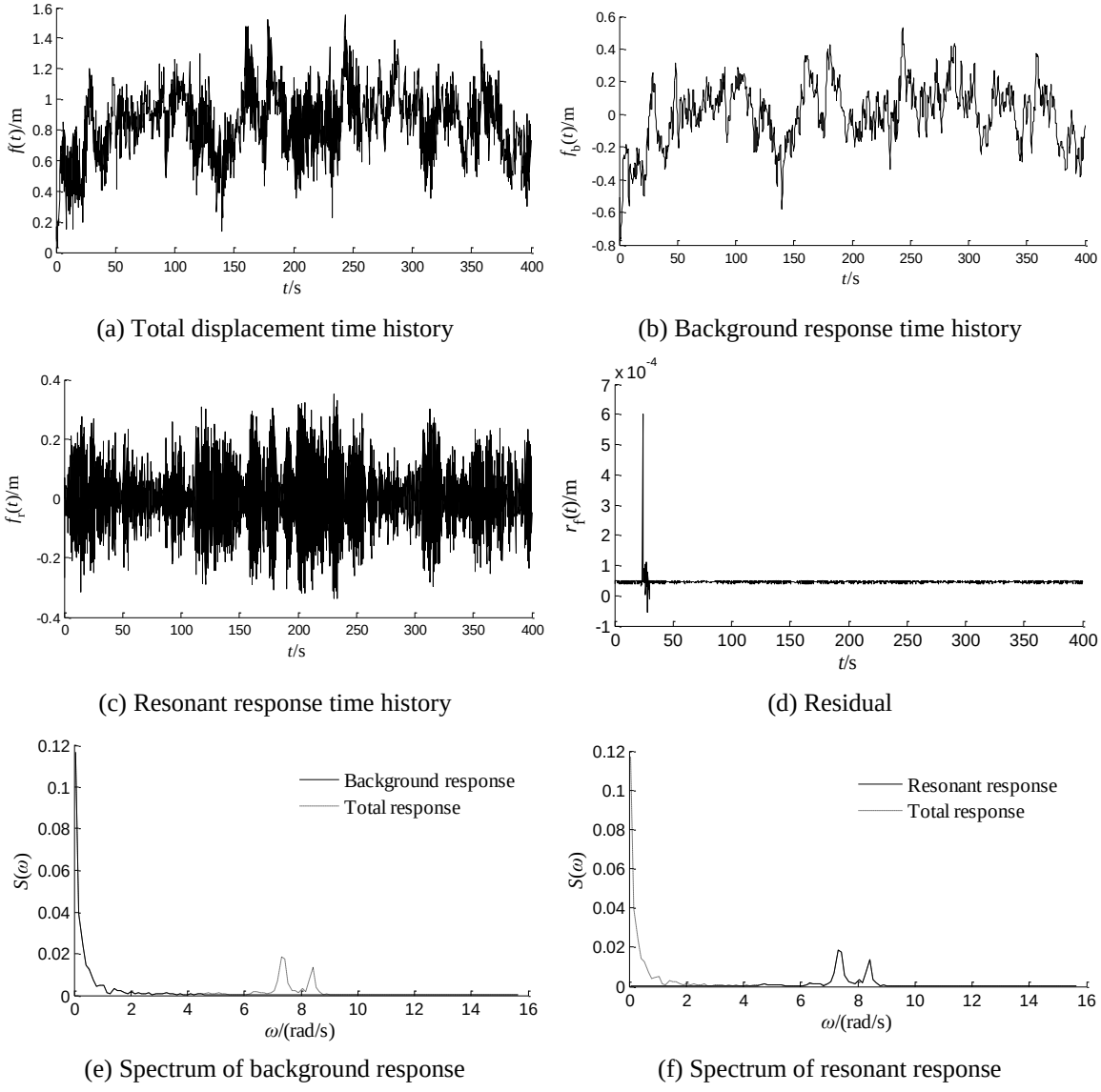

(a) Total displacement time history

(b) Background response time history

(c) Resonant response time history

(d) Residual

(e) Spectrum of background response

(f) Spectrum of resonant response

Fig. 8 Separation of background and resonant response time histories and verifications of residual and power spectra for typical node NU

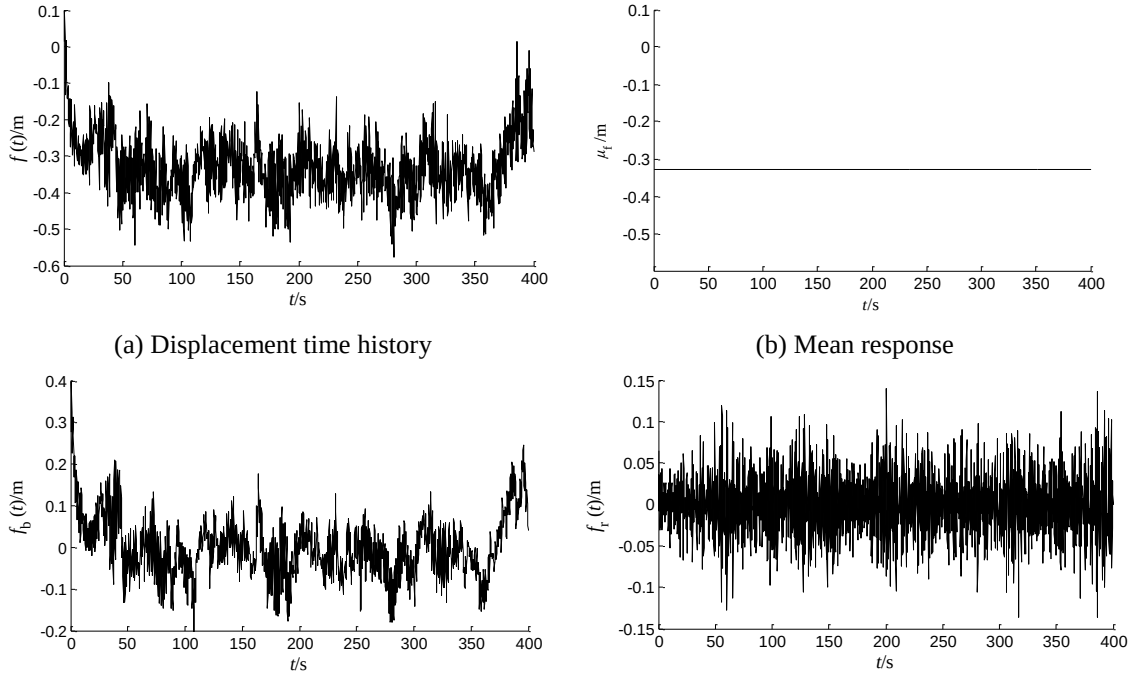

(a) Displacement time history (b) Mean response

(c) Background response time history (d) Resonant response time history

Fig. 9 Displacement time history of typical node TR and its background and resonant components

9. Conclusions

The time-domain method is applicable for wind-induced dynamic response analysis of flexible structures. For large-span structures, the power spectral analysis of a large number of response signals is required. On the other hand, it is difficult for implementation of the time-domain method to separate the background and resonant response time histories from each other. Through the research work of this paper, it is found that the wavelet packet transform can be applied for accurate and efficient computation of power spectra of response signals. Also, taking advantage of the time-frequency transform, the background and the resonant response time histories are extracted successfully from the total-response signal.

In this paper, the essential linkage between wavelet packet analysis and power spectrum is revealed by derivation of equations. On this basis, a new approach is proposed for power spectral computation of wind-induced response and separation of background response from resonant response. Also, verification criteria of power spectrum are proposed. Further, an engineering example is adopted to illustrate the proposed approach. The conclusions can be summarized as follows.

(1) The frequency range of a signal can be finely divided using the wavelet packet transform to realize the uniform high resolution in the whole frequency range. For the determinative signals, the frequency components contained in the signal are detected accurately and distinguished clearly even if they are very close in value.

(2) For the wind-induced response signal (stochastic signal), it is proved by the two criteria that

the power spectral curve obtained by the proposed approach truly describes the rules of energy distribution of the signal, which indicates the high accuracy of the power spectrum. Meanwhile, the application of Mallat's fast algorithm in wavelet packet decomposition ensures the high efficiency of computation. Because the proposed approach is both accurate and efficient, it is advantageous for power spectral analysis of various responses of large-span flexible structures.

(3) When the wavelet packet transform is used to compute the power spectrum of the signal, the information in time-domain is still retained taking advantage of the time-frequency transform of wavelet packet analysis. Therefore the wavelet packet analysis of the structural response signal is an effective approach to separation of background and resonant response time histories.

(4) Both the background response and the resonant response are not negligible for large-span flexible structures. The ratio of background/resonant variance to total variance varies with the response type. The numerical results show that the background response is larger than the resonant response for large-span cable-membrane structures, and the wind-induced response has the features of wide band and forced vibration.

(5) The background response time history reflects the variational tendency of the zero-mean fluctuating response with time and has the low-frequency and nonstationary feature. In contrast, the resonant response time history has the high-frequency and stationary feature.

Acknowledgments

This research was financially supported by the National Natural Science Foundation of China (Grant Nos. 51208116 and 51178121) and the Guangdong Natural Science Foundation of China (Grant Nos. S2011040004060 and S2012020011082).

References

Aksoy, H., Toprak, Z.F. and Aytek, A. (2004), "Stochastic generation of hourly mean wind speed data", *Renew. Energy*, **29**, 2111-2131.

Chen, X. and Zhou, N. (2007), "Equivalent static wind loads on low-rise buildings based on full-scale pressure measurements", *Eng. Struct.*, **29**(10), 2563-2575.

Clough, R.W. and Penzien, J. (2003), *Dynamics of Structures*, Third Edition, Computers & Structures, Inc., Berkeley, CA, USA.

Holmes, J.D. (2002), "Effective static load distributions in wind engineering", *J. Wind Eng. Indus. Aerodyn.*, **90**, 91-109.

Kitagawa, T. and Nomura, T. (2003), "A wavelet-based method to generate artificial wind fluctuation data", *J. Wind Eng. Indus. Aerodyn.*, **91**, 943-964.

Li, Y.X., Yang, Q.S. and Tian, Y.J. (2011), "Background response equivalent static wind load of large-span roofs based on energy equation", *Appl. Mech. Mater.*, **99-100**, 338-341.

Mitra, S.K. (2001), *Digital Signal Processing-A Computer-Based Approach*, Second Edition, English Reprinted Edition, Tsinghua University Press, Beijing, China.

Percival, D.B. and Walden, A.T. (2000), *Wavelet Methods for Time Series Analysis*, Cambridge University Press, Cambridge, England.

Terradellas, E. and Morales, G. (2001), "Wavelet methods: application to the study of the stable atmospheric boundary layer under non-stationary conditions", *Dyn. Atmos. Ocean.*, **34**, 225-244.

Wacker, J. (2004), *Wind tunnel tests for determination of the main carrying structures and the membrane roof of the Foshan stadium under quasi-static and dynamic wind loads*, Wind Tunnel Experiment Report,

Wacker of Engineers, Birkenfeld, Germany. (in German)
Wu, Y., Sun, X.Y. and Shen, S.Z. (2008), "Computation of wind-structure interaction on tension structures", *J. Wind Eng. Indus. Aerodyn.*, **96**(10-11), 2019-2032.
Yang, Q., Chen, B., Wu, Y. and Tamura, Y. (2013), "Wind-induced response and equivalent static wind load of long-span roof structures by combined Ritz-proper orthogonal decomposition method", *J. Struct. Eng.*, **139**(6), 997-1008.
Zhou, X.Y. and Gu, M. (2010), "An approximation method for computing the dynamic responses and equivalent static wind loads of large-span roof structures", *Int. J. Struct. Stab. Dyn.*, **10**(5), 1141-1165.

CC